Journal of Education for Humanities

A peer-reviewed quarterly scientific journal issued by College of Education for Humanities / University of Mosul

Deriving SPI from Satellite-Based CHIRPS Daily Precipitation Using Google Earth Engine for Drought Monitoring in Iraq

Khudhur Rasheed Abdulrahman [1]

Department of Geography, College of Education for Humanities, University of Mosul, Mosul, Ninavah, Iraq [1]

Article information

Received : 19/1/2026
Revised 26/2/2026
Accepted : 4/3/2026
Published 1/9/2026

Keywords:

SPI · Drought · CHIRPS · Precipitation · GEE · Iraq

Correspondence:

Khudhur Rasheed

khder.rasheed@uomosul.edu.iq

Abstract

The phenomenon of drought is one of the most persistent hydroclimatic hazards affecting arid and semiarid regions and Iraq is highly vulnerable as it is highly dependent on winter precipitation with limited continuous ground-based observational data. Despite a noticeable increase in the literature on drought in the Middle East, thorough long-term and spatially explicit assessments of meteorological drought in Iraq are rather limited; previous studies largely rely on station-based analyses limited in spatial extent or on short term data sets that poorly reflect multiperiod variability.

To fill this gap, the current study assesses meteorological drought in Iraq using the Standardized Precipitation Index (SPI) based on satellite-based CHIRPS Daily Precipitation data that was assimilated within the Google Earth Engine (GEE) platform. SPI calculations were performed at 3, 6, and 12-month accumulation scales for 41 water years (1983/84-2023/24), which also ensured that calculations followed the dynamics of water years in the region. The study adopted a two combined approach (i) a nationally aggregated SPI time series to characterize temporal variability, trends, and multi-year phases with (ii) spatially explicit SPI-12 (September) class mapping to quantify areal extent and long-term drought/wetness frequency.

The results show strong expeditionary yearly by distinctive dry and wet regimes. The water years 2007/08 represents the most severe long-term drought signal (SPI-12 Sep = -2.19), while the water year 2018/19 marks an extreme wet episode (SPI-12 Sep = +3.52), during which extreme wetness covered (94.5%) of Iraq (412,000 km2). Frequency analysis indicates that annual conditions are concentrated near neutrality (SPI-12 Sep: mild wet 39% and mild drought 34%), whereas extreme classes are rare (=2% each for extreme drought and extreme wetness). Spatial frequency patterns highlight higher drought occurrence in western and southwestern Iraq and more frequent wet conditions in the northeastern mountainous region, reflecting Iraq's climatic gradient.

Overall, the integration of CHIRPS Daily precipitation with cloud-based processing provides a reproducible and operational drought-monitoring framework suitable for data-scarce regions, offering valuable support

DOI: ************,,

مجلة التربية للعلوم الانسانية

مجلة علمية فصلية محكّمة، تصدر عن كلية التربية للعلوم الإنسانية / جامعة الموصل

اشتقاق مؤشر الهطول المعياري (SPI) من بيانات الأمطار اليومية المعتمدة على الأقمار الصناعية (CHIRPS) باستخدام Google Earth Engine لرصد الجفاف في العراق

خضر رشيد عبدالرحمن [1]

قسم الجغرافيا، كلية التربية للعلوم الإنسانية، جامعة الموصل، الموصل، نينوى، العراق [1]

معلومات الارشفة

تاريخ الاستلام : 19/1/2026

تاريخ المراجعة : 26/2/2026

تاريخ القبول : 4/3/2026

تاريخ النشر : 2026/9/1

الكلمات المفتاحية :

مؤشر الهطول المعياري، الجفاف، CHIRPS، الأمطار، GEE، العراق

معلومات الاتصال

خضر رشيد

khder.rasheed@uomosul.edu.iq

الملخص

تُعدّ ظاهرة الجفاف من أكثر الأخطار الهيدرو-مناخية استمراراً وتأثيراً في الأقاليم الجافة وشبه الجافة، ويُعدّ العراق من البلدان شديدة الهشاشة تجاهها لاعتماده الكبير على الأمطار الشتوية مع محدودية البيانات الرصدية الأرضية المستمرة. وعلى الرغم من الزيادة الملحوظة في الأدبيات العلمية المتعلقة بالجفاف في منطقة الشرق الأوسط، فإن التقييمات طويلة الأمد وذات التمثيل المكاني التفصيلي للجفاف الأرصادي في العراق ما تزال محدودة؛ إذ اعتمدت معظم الدراسات السابقة على تحليلات قائمة على محطات رصد ذات نطاق مكاني محدود، أو على مجموعات بيانات قصيرة الأمد لا تعكس بصورة كافية التباين متعدد الفترات.

لسد هذه الفجوة، تُقيِّم هذه الدراسة الجفاف الأرصادي في العراق باستخدام مؤشر الهطول المعياري (SPI) بالاعتماد على بيانات الأمطار اليومية المعتمدة على الأقمار الصناعية (CHIRPS)، والتي جرى دمجها ومعالجتها ضمن منصة Google Earth Engine (GEE). أُجريت حسابات SPI على مقاييس تجميع 3 و6 و12 شهراً، ولـ 41 سنة مائية (24/2023–84/1983)، بما يضمن اتساق الحسابات مع ديناميكية السنوات المائية في المنطقة. اعتمدت الدراسة منهجًا مركّبًا من جزأين: (1) بناء سلسلة زمنية وطنية مُجمَّعة لمؤشر

الهطول المعياري (SPI) على مستوى العراق بهدف وصف التغيّر الزمني للجفاف، وبيان الاتجاهات العامة، وتحديد الفترات الممتدة (عدة سنوات) التي تسود فيها ظروف الجفاف أو الرطوبة؛ و(2) إعداد خرائط مكانية تفصيلية لتصنيفات SPI-12 عند نهاية شهر أيلول/سبتمبر لقياس مدى اتساع الجفاف أو الرطوبة على مساحة العراق، وحساب تكرار فئاتهما على المدى الطويل.

وتُظهر النتائج وجود تذبذب سنوي واضح في الجفاف والرطوبة مع تعاقب فترات جافة وأخرى رطبة بصورة مميزة. وقد سُجلت السنة المائية 08/2007 بوصفها أشد حالة جفاف طويل الأمد (SPI-12 في أيلول = −2.19)، في حين مثّلت السنة المائية 19/2018 حالة رطوبة متطرفة (SPI-12 في أيلول = +3.52)، إذ غطّت فئة "الرطوبة المتطرفة" نحو 94.5% من مساحة العراق (قرابة 412,000 كم²). كما تُبيّن تحليلات التكرار أن أغلب السنوات تقع قريبًا من الحالة الاعتيادية (SPI-12 في أيلول: رطوبة خفيفة 39%، وجفاف خفيف 34%)، بينما تبقى الحالات المتطرفة قليلة الحدوث (نحو 2% لكل من الجفاف المتطرف والرطوبة المتطرفة). وتوضح خرائط التكرار المكاني أن فرص تكرار الجفاف أعلى في غرب وجنوب غرب العراق، في حين تتكرر الظروف الرطبة أكثر في المناطق الجبلية شمال شرق البلاد، وهو ما يعكس التدرّج المناخي المعروف في العراق من مناطق قليلة المطر غربًا إلى مناطق أعلى مطرًا شمال شرقًا.

بصورة عامة، يوفّر دمج بيانات الأمطار اليومية من CHIRPS مع المعالجة السحابية إطاراً عملياً وقابلًا للتحقق وإعادة التطبيق لرصد الجفاف، وهو ملائم للأقاليم الشحيحة بالبيانات، ويقدّم دعماً علمياً قيّماً لإدارة الموارد المائية والتخطيط المناخي

DOI: ************,

1. Introduction

Drought is a major hydroclimatic hazard in arid and semi-arid regions such as Iraq. For meteorological drought assessment, the Standardized Precipitation Index (SPI) is widely used because it relies only on precipitation and can be computed at multiple accumulation timescales (e.g., 3, 6, and 12 months). Foundational guidance for SPI calculation and interpretation is provided by WMO (2012) and the original AMS conference paper by McKee et al. (1993).

Recent advances in cloud geospatial computing enable efficient, reproducible analysis of long climatic time series; Google Earth Engine (GEE) is widely adopted for large-scale geospatial processing and transparent workflows (Gorelick et al., 2017) .Among satellite-derived precipitation datasets, CHIRPS provides quasi-global daily precipitation since 1981 at ~0.05° spatial resolution, integrating satellite infrared information with station observations, which is particularly valuable where gauge networks are sparse.

Recent advances in cloud geospatial computing enable efficient, reproducible analysis of long climatic time series; Google Earth Engine (GEE) is widely adopted for large-scale geospatial processing and transparent workflows (Gorelick et al., 2017). Among satellite-derived precipitation datasets, CHIRPS provides quasi-global daily precipitation since 1981 at ~0.05° spatial resolution, integrating satellite infrared information with station observations, which is particularly valuable where gauge networks are sparse (C. Funk et al., 2015).

The main aims of this study are to determine Standardized Precipitation Index (SPI) from CHIRPS Daily data in Google Earth Engine (GEE) platform at several timescales (3, 6 and 12 months). The study will examine the spatiotemporal patterns of drought in Iraq between the years 1984-2024. This will emphasize the inter-annual variability related to severity and frequency focusing on the most vulnerable regions in the country. Finally, the study is directed to achieve a replicable and nationally applicable scheme of drought monitoring via open-access satellite observations and cloud computing tools.

Several studies in Iraq and the broader Middle East have utilized CHIRPS to monitor drought through SPI. In Iraq Ahmad et al. (2021) assessed the spatiotemporal variability of meteorological droughts in northern Iraq using CHIRPS data (1981–2018), demonstrating that SPI derived from CHIRPS successfully captured major drought periods and regional variability. Suliman et al. (2024) evaluated the accuracy of different satellite-based precipitation products (APHRODITE and CHIRPS) for meteorological drought assessment. Their findings highlighted the strong performance of CHIRPS, further validating its application in environments with limited in-situ data.

At the global level, the CHIRPS serves as a popular tool which scientists use to monitor drought conditions across the entire world. In China, the study by Wu et al. (2019) assessed CHIRPS performance through which the product demonstrated suitable drought pattern detection but needed separate testing for each geographic area because of its variable performance across different regions. In India, Pazhanivelan et al. (2023) compared multiple satellite rainfall products, including IMERG, TRMM, PERSIANN, and CHIRPS, in Tamil Nadu. The research showed that CHIRPS provides dependable SPI-based drought monitoring data which functions properly during monsoon periods. Across Africa, several studies in Ethiopia, such as those by Dejene et al. (2023) and Shalishe et al. (2022), showed that CHIRPS data combined with SPI information enables drought monitoring in regions which do not have ground-based measurement stations or with sparse in-situ networks.

The SPI workflows for large scale drought monitoring need to be standard and reproducible. UN-SPIDER (2025) and UNCCD (2025) support this through their recommendation of using CHIRPS data in Google Earth Engine. C. Funk et al. (2015) explained how CHIRPS was created by combining satellite data with weather station information on the ground. Some researchers like Gorelick et al. (2017), who introduced the planetary-scale capabilities of GEE that have facilitated the application of SPI across wide spatial and temporal domains.

Collectively, these global studies demonstrate that combining CHIRPS data with SPI has become an established approach for drought monitoring across diverse regions in Asia, Africa, and Latin America. At the same time, the adoption of GEE has significantly accelerated computations and streamlined workflows, enabling the production of accurate, operational drought maps at both national and regional scales. However, reveal some limitations. Most previous works in Iraq have focused on specific sub-regions (north or south) or shorter timeframes, and only a Few have applied the methodology comprehensively across the entire country within a long-term framework (Base line and analysis 41 water year), particularly using cloud- computing platforms such as Google Earth Engine.

The present study addresses these gaps by covering the entire territory of Iraq over a long-term period (1984-2024) in addition to deriving SPI from CHIRPS Daily data exclusively within GEE ensuring reproducibility and scalability, as well as providing a multi-scale assessment (3, 6, 12 months) of drought dynamics, offering a comprehensive picture of severity, duration, and frequency. Also, delivering high-resolution spatiotemporal drought maps to support national-level water and agricultural policy-making.

By doing so, this study contributes a novel, replicable, and operational framework for drought monitoring in Iraq using open-access satellite data and cloud computing.

2. Study Area and Data

2.1 Study Area

The study area is defined by the political boundaries of the Republic of Iraq, which covers an area of 437,072 km². Geographically, Iraq is located in the southwestern part of Asia and is bordered by five countries: Turkey to the north, Iran to the east, and Kuwait to the south, while to the west it shares borders with Saudi Arabia, Jordan, and Syria. Astronomically, Iraq extends between latitudes 37°22′50″ N - 29°5′20″ N, and longitudes 38°45′55″ E - 48°45′35″ E (Fig.1 a).

Iraq climate is characterized by hot and dry summers (June-September) and cool and wet winters (November-March). Majority of the annual rainfall occurs during the winter months, while the summer is extremely dry. The rainfall amount varies geographically, the mountainous northeastern part of the country experiences between 400 millimeters (mm) and 1,000 mm of annual precipitation, whereas the desert regions only receive around 50 mm to 200 mm. The transitional area between the mountains and the desert experiences around 200 mm to 400 mm of annual rainfall (International Energy Agency (IEA), 2025). the average annual temperature across Iraq is around 22 °C, but varies from as low as 8°C in the high mountains to as high as 28°C in the hot and dry southern desert. Minimum temperatures in the north can be below zero in the winter months, while maximum temperatures in the south can exceed 45°C regularly through the summer months (RCCC, 2024).

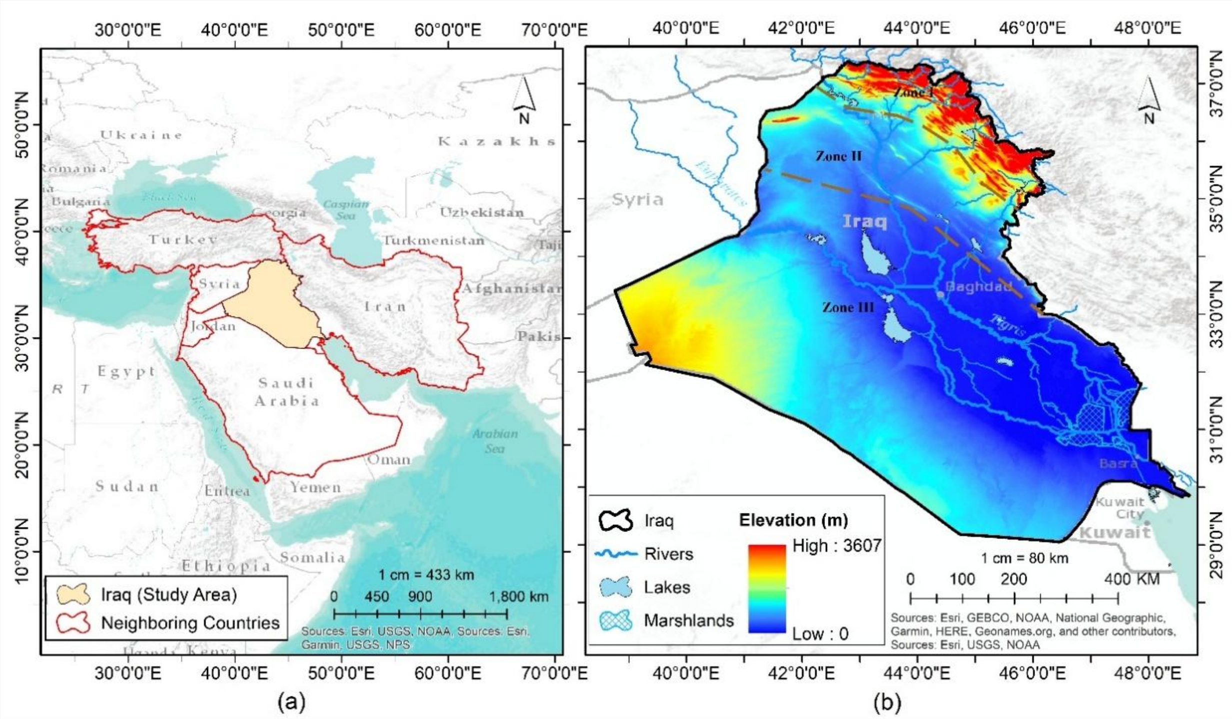

Fig. 1 Study Area. Map (a) illustrates the geographical location of Iraq and its political boundaries within Southwest Asia, while map (b) presents the topographical gradient and the main climatic divisions according to the Koppen classification, including the distribution of rivers, lakes, and marshes.

Koppen climate classifications divide the study area into three zones: is predominantly subtropical desert (BWh) climate for zone III which is dominates the parts of the country, followed by subtropical steppe (BSh) and dry-summer subtropical (Ca) climates for zones I and II (Fig. 1 b). The combination of low rainfall and extreme temperatures has resulted in the majority of the country being arid. Consequently, Iraq frequently faces natural disasters such as severe droughts due to its high climate variability (Salman et al., 2020).

2.2 CHIRPS Precipitation Data

Since 1999, U.S. Geological Survey (USGS) and Climate Hazards Center (CHC) scientists at University of California, Santa Barbara (UCSB)—supported by funding from U.S. Agency for International Development (USAID), The National Aeronautics and Space Administration(NASA) and National Oceanic and Atmospheric Administration (NOAA)—have developed techniques for producing rainfall maps, especially in areas where surface data is sparse and CHIRPS one of them (Funk et al., 2014).

The Climate Hazards group Infrared Precipitation with Stations (CHIRPS) dataset builds on previous approaches to 'smart' interpolation techniques and high resolution, long period of record precipitation estimates based on infrared Cold Cloud Duration (CCD) observations (Funk et al., 2012). The algorithm i) is built around a 0.05° climatology that incorporates satellite information to represent sparsely gauged locations, ii) incorporates daily, pentadal, and monthly 1981- present 0.05° CCD-based precipitation estimates, iii) blends station data to produce a preliminary information product with a latency of about 2 days and a final product with an average latency of about 3 weeks, and iv) uses a novel blending procedure incorporating the spatial correlation structure of CCD-estimates to assign interpolation weights (Funk et al., 2015).

The "CHIRPS Daily: Climate Hazards Center InfraRed Precipitation With Station Data (Version 2.0 Final)" dataset, developed and provided by the University of California, Santa Barbara (UCSB) and the Climate Hazards Group (CHG), was employed in this study through the Google Earth Engine platform. This dataset offers daily precipitation records covering the period from 1981-01-01 to the present, with a spatial resolution of 0.05° (~5.6 km at the equator) .

For the purpose of this study, the analysis was conducted using water years (October to September) covering 41 complete water years (1983/1984–2023/2024), extracted and processed entirely within Google Earth Engine (Fig. 2). This approach ensures consistency with hydrological cycles in Iraq and provides a robust and reliable basis for calculating the SPI.

The CHIRPS dataset was chosen because it combines satellite-derived precipitation estimates with ground station observations, providing long-term, high-resolution, and spatially consistent rainfall data that is particularly suitable for drought monitoring in data-scarce regions such as Iraq. Fig. 2 presents the monthly mean precipitation over Iraq based on CHIRPS during the period Oct 1983 – Sep 2024.

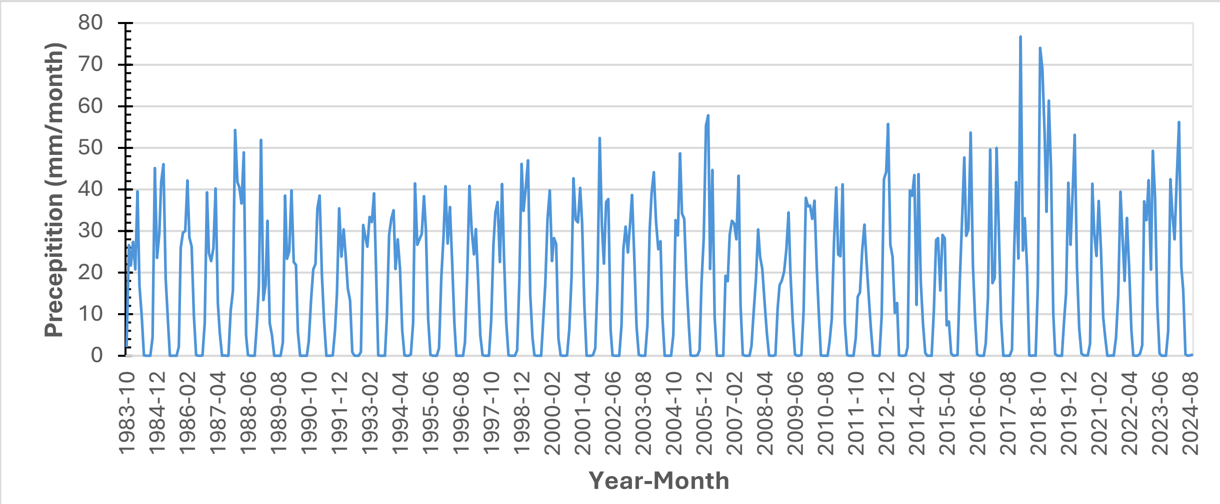

Fig. 2 Monthly Time Series of the Mean Precipitation over Iraq based on CHIRPS for Water Years 1983/84 – 2023/24

3. Methods

3.1 Standardized Precipitation Index (SPI)

Several indices have been employed to assess drought globally. Many researchers have utilized the Surface Water Supply Index (SWSI) to evaluate hydrological fluctuations (Dezman et al., 1983; Khan et al., 2018; Kim et al., 2012). However, due to its complexity, it is not widely applied. While the Palmer Drought Severity Index (PDSI) is a commonly used indicator for drought assessment (Palmer, 1965), one of its main limitations lies in its lack of comparability across different regions, as it is highly dependent on local climatic characteristics (Mares et al., 2016; Mo et al., 2017).

The Palfai Aridity Index (PAI) is another indicator used in Southeastern European countries (Pálfai, 2002). Alongside these, other indices such as the Decile Index, the Crop Moisture Index (CMI) (Morid et al., 2006), the Reconnaissance Drought Index (RDI) (Tsakiris et al., 2007),the Rainfall Anomaly Index (RAI) (Van-Rooy, 1965), and the Atmospheric Crop Moisture Index (Uang-aree et al., 2017) are also employed for drought monitoring. Moreover, many researchers have utilized remote sensing datasets for drought (AghaKouchak et al., 2015; Liu et al., 2023; Muthumanickam et al., 2011; Wei et al., 2021).

These various indices prove useful for particular applications yet they contain multiple major drawbacks which include their need for local weather data and their absence of standardized methods and their complicated measurement procedures that make them unsuitable for large-scale time-based and geographical assessments. The Standardized Precipitation Index (SPI) serves as the primary drought assessment tool because it provides simple operation and suits different time spans and enables scientists to analyze drought patterns across different climate regions.

The Standardized Precipitation Index (SPI), proposed by McKee et al. (1993), is one of widely used meteorological drought index, which is also recommended by the World Meteorological Organization (WMO) (Mukama et al., 2025) was employed in this study due to its numerous advantages. The SPI index operates with precipitation data as its only requirement because it does not need multiple climatic and hydrological variables which makes it suitable for areas with missing meteorological or hydrological data.

The Standardized Precipitation Index (SPI) serves to measure precipitation deficits which occur at different time spans. The SPI-1 index enables scientists to determine the severity of meteorological drought, but SPI-3 indexes help them understand agricultural drought severity and SPI-12 to SPI-24 indexes track hydrological drought (Zhang et al.,2023). The 1-month SPI (SPI-1) compares total monthly precipitation from a particular year to all monthly precipitation data in the climatological record to detect short periods of water imbalance which result in meteorological drought. The 3-month SPI (SPI-3) evaluates total precipitation from a three-month period against historical records of the same time frame to identify moderate changes in moisture levels which help evaluate seasonal rainfall patterns. The 6-month SPI (SPI-6) measures precipitation that occurs during six months which follow each other in sequence relative to historical climate patterns to show how seasonal rainfall affects hydrological systems. The 12-month up to 24-month SPI (SPI-12 up to SPI-24) evaluates yearly precipitation totals against their corresponding historical data to detect extended periods of abnormal hydrological conditions which affect groundwater replenishment and river discharge and drought severity (Kumanlioglu, 2020).

The Standardized Precipitation Index (SPI) operates by normalizing precipitation data through a probability distribution function, thereby expressing SPI values as standard deviations from the median normalization enables SPI to estimate both dry and wet periods on a comparable scale. Accumulated values over various intervals are used to assess drought magnitude or severity. A minimum of 30 years of continuous monthly precipitation records is typically required, with longer records preferred to improve reliability. Care should be exercised when using the SPI for timescales of less than one month or longer than 24 months, due to potential statistical unreliability (WMO, 2012). As SPI interpretation is spatially-invariant, uniform thresholds are used in disparate regions. Its probability-based formulation -transforming observed precipitation probabilities into standardized index values- makes it especially suited for risk management and decision-making triggers (Gumus, 2023).

When SPI values range from 0 to –0.99, the condition is classified as "mild drought"; values between –1.0 and –1.49 are categorized as "moderate drought"; values between –1.5 and –1.99 are considered "severe drought"; and values less than or equal to –2.0 are classified as "extreme drought" (Table 1).

Table 1 SPI classification

SPI Value	Category	Symbol
$SPI \leq -2.0$	Extremely drought	ED
$-1.99 < SPI < -1.5$	Severely drought	SD
$-1.49 < SPI < -1.0$	Moderately drought	MD
$0 > SPI > -0.99$	Mild drought	ND
$0.99 > SPI > 0$	Mild wet	NW
$1.49 > SPI > 1$	Moderately wet	MW
$1.99 > SPI > 1.5$	Severely wet	SW
$SPI \geq 2.0$	Extremely wet	EW

In this study the Standardized Precipitation Index (SPI) was computed by fitting 41 water years (1983/84-2023/24) of CHIRPS precipitation data into a gamma probability distribution function using Eq. (1) (Stagge et al., 2015).

$$g(x) = \frac{1}{\beta^{\alpha}\Gamma(\alpha)} x^{\alpha-1} e^{-\frac{x}{\beta}} \quad \text{for } x > 0 \tag{1}$$

Where x is the amount of precipitation, α and β are the shape and scale parameters respectively and Γ(α) is the is the gamma function defined by Eq. (2).

$$\Gamma(\alpha) = \int_0^x x^{a-1} e^{-x} dy \tag{2}$$

The best values of α and β are estimated by the maximum likelihood method using Eq. (3).

$$\alpha = \frac{1}{4A}\left(1 + \sqrt{1 + \frac{4A}{3}}\right), \beta = \frac{\bar{x}}{a}, \text{where } A = \ln(\bar{x}) - \frac{\sum \ln x}{n} \tag{3}$$

Where $\bar{x}$ and n are the mean and the number of precipitation observations respectively, x is the quantity of precipitation in the sequence of data. and A is the sample statistic.

The cumulative probability for a given month can be obtained by using Eq. (4)

$$G(x) = \int_0^x g(x)dx = \frac{1}{\beta^\alpha \Gamma(\alpha)} \int_0^x x^{a-1} e^{-\frac{x}{\beta}} dx \tag{4}$$

Values obtained from the cumulative probability G(x) were subsequently converted into standardized values using Eqs. (5) by employing the approximation technique developed by Abramowitz & Stegun (1967).

$$z = SPI = \begin{cases} -\left(t - \dfrac{C_0 + C_1 t + C_2 t^2}{1 + d_1 t + d_2 t^2 + d_3 t^3}\right) & 0 < H(x) \le 0.5 \\ +\left(t - \dfrac{C_0 + C_1 t + C_2 t^2}{1 + d_1 t + d_2 t^2 + d_3 t^3}\right) & 0.5 < H(x) \le 1 \end{cases} \tag{5}$$

$$t = \begin{cases} \sqrt{\ln\left(\dfrac{1}{(H(x))^2}\right)} & 0 < H(x) \le 0.5 \\ \sqrt{\ln\left(\dfrac{1}{(1 - H(X))^2}\right)} & 0.5 < H(x) \le 1 \end{cases} \tag{6}$$

Where: $H(x) = q + (1 - q)G(x)$, q is s the probability of zero rainfall with constants $C_0 = 2.515517$, $C_1 = 0.802853$, $C_2 = 0.010328$, $d_1 = 1.432788$, $d_2 = 0.189269$ and $d_3 = 0.001308$.

In this study the Standardized Precipitation Index (SPI) was computed using two complementary approaches to ensure both temporal comparability and spatial representativeness. All calculations were implemented in the Google Earth Engine (GEE) platform using daily precipitation data from the Climate Hazards Group InfraRed Precipitation with Station Data (CHIRPS v2.0) at a spatial resolution of 0.05° (~5.6 km). The analysis was aligned with hydrological years (October–September), and the baseline period for distribution fitting was set to 1983/84–2023/24. SPI was computed for the following accumulation windows: SPI-3 for end-months December, March, June, and September. SPI-6 for end-months March and September. SPI-12 for the end-month September.

3.1.1 Aggregate-first (DrinC-style) approach

In the first approach, Monthly precipitation totals were aggregated over all CHIRPS grid cells covering Iraq to construct a single national time series (Fig 2). For instance, the October 1983 national precipitation value was computed by first summing the daily CHIRPS precipitation at each grid cell to obtain monthly totals (Fig. 3), and then taking the spatial mean of these grid-cell totals over Iraq, and the same procedure was applied to all subsequent months of each year. This procedure yielded a continuous monthly precipitation series for the entire country from October 1983 to September 2024 (Fig. 2).

The national precipitation series was then used to calculate SPI values for the different accumulation windows (SPI-3, SPI-6, SPI-12). The statistical computation followed the Gamma distribution fitting with the Thom Maximum Likelihood Estimation (Thom-MLE) method (THOM, 1958), explicitly treating zero-precipitation months (q-zero). The fitted cumulative distribution was subsequently transformed into the standard normal distribution using the inverse error function, yielding standardized SPI values with mean zero and variance one(McKee et al., 1993). This procedure reproduces the logic of the DrinC software and ensures direct comparability with widely used drought indices in the literature (Tigkas et al., 2015). This approach was used in Section 4.1 and 4.2 of this study.

3.1.2 Pixel-based approach

In the second approach, the same statistical procedure was applied independently to each 0.05° CHIRPS grid cell across Iraq. For every pixel, monthly and multi-month precipitation totals were computed from the daily CHIRPS data, fitted to the Gamma distribution using the Thom Maximum Likelihood Estimation (Thom-MLE) with explicit q-zero correction, and then transformed into standardized SPI values. This yielded spatially explicit SPI fields for each accumulation window (SPI-3, SPI-6, SPI-12), capturing the spatial heterogeneity of drought and wetness conditions across the country.

These pixel-based SPI fields form the basis of the spatial and areal analyses presented in Section 4.3. First, annual areas of each drought and wetness class (ND, MD, SD, ED and NW, MW, SW, EW) were computed by counting the number of pixels in each category and converting them into square kilometers and percentages of Iraq's land area. Second, the same gridded SPI classifications were used to derive composite areal indices DI and WI (Eq. 7 and Eq. 8) and to construct drought and wetness frequency maps for the driest and wettest water years at SPI-3 and SPI-6, as well as the long-term frequency of dry and wet years at SPI-12. In this way, the pixel-based approach provides the spatially resolved information needed to quantify the areal extent, persistence and geographic distribution of SPI classes across Iraq, complementing the national-scale time-series analysis obtained from the aggregate-first approach.

$$\mathrm{DI}_k(y) = \frac{1}{n}\sum_{w=1}^{n} A_{dry}(y, w) \tag{7}$$

$$\mathrm{WI}_k(y) = \frac{1}{n}\sum_{w=1}^{n} A_{wet}(y, w) \tag{8}$$

Where:

$\mathrm{DI}_k(y)$: Composite aridity index for water year y at SPI timescale k months (in km^2).

$\mathrm{WI}_k(y)$: Composite wetness index for water year y at SPI timescale k months (in km^2).

n: Number of SPI windows used during the year (e.g., 4 for SPI-3, 2 for SPI-6 and 1 for SPI-12).

$A_{dry}(y, w)$: Area classified as dry (categories ND–ED) in window w of year (in km^2).

$A_{wet}(y, w)$: Area classified as wet (categories NW–EW) in window w of year (in km^2).

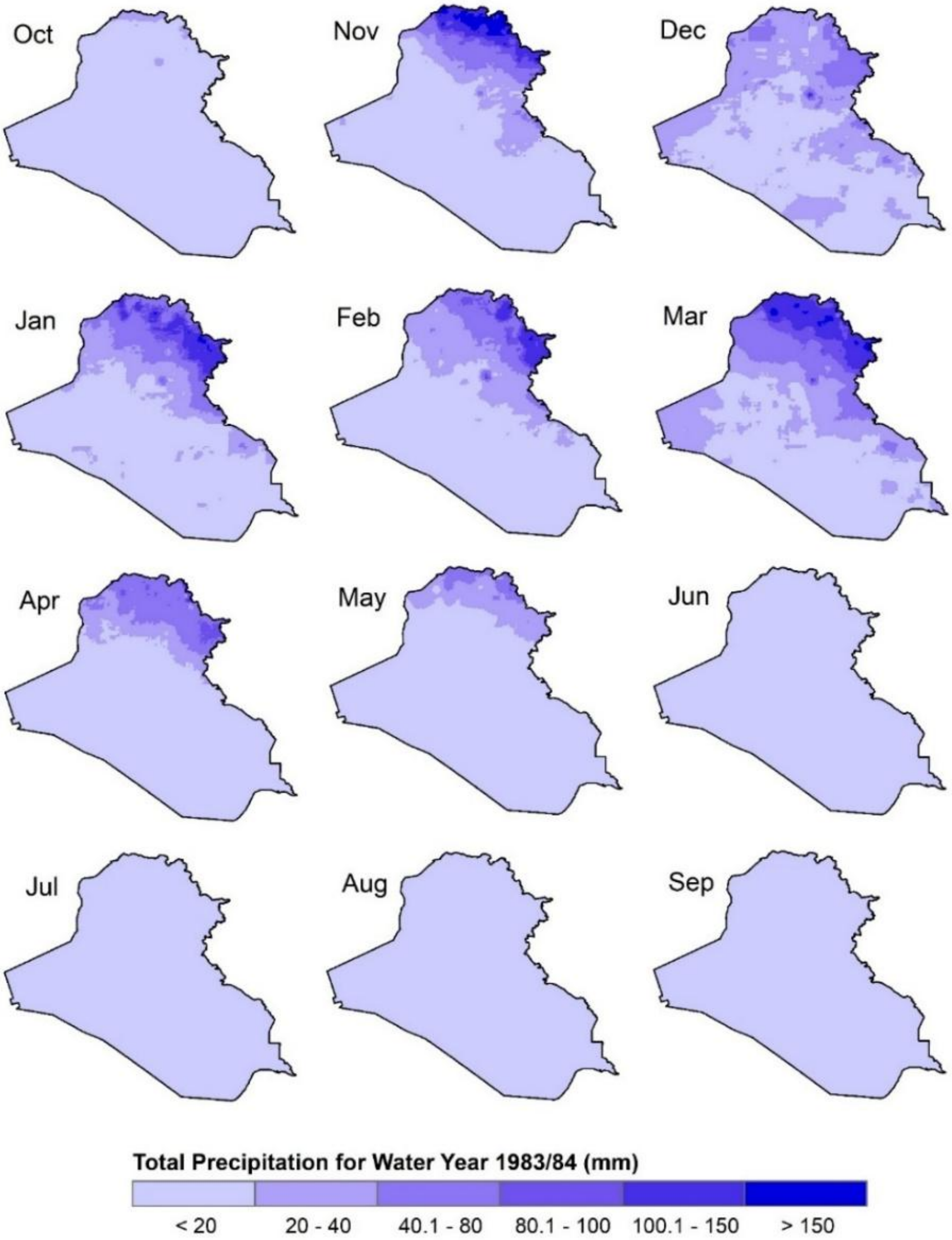

Fig. 3 Monthly precipitation totals over Iraq for water year 1983/84 derived from CHIRPS. Each panel shows the spatial distribution of monthly accumulated

precipitation (mm) for one month of the 1983/84 water year, from October 1983 (top left) to September 1984 (bottom right). Higher values are concentrated over northern Iraq, especially during the winter and early spring months.

4. Results and Discussion

4.1 Temporal variation of drought

The Standardized Precipitation Index (SPI) time series reflects a clear fluctuation in drought/wetness intensity over the period 1983/84–2023/24. Fig. 4 shows the SPI-3 trajectories for four seasonal windows (Dec, Mar, Jun, Sep), while Fig. 5 presents the SPI-6 behavior for the window pair (Mar, Sep). The dashed gray line in all figures represents the five-year moving average; it reduces short-term noise and highlights the overall trends.

4.1.1 Short-term (SPI-3)

The 3-month Standardized Precipitation Index (SPI-3) is calculated from precipitation accumulated over a three-month period and then standardized relative to the long-term climatological distribution of the national precipitation series for Iraq. This timescale primarily captures short-term to seasonal anomalies in rainfall and is therefore widely used to monitor meteorological and agricultural drought, because it is closely linked to soil-moisture conditions and the water available to crops during a growing season (World Meteorological Organization (WMO), 2012). In this study, SPI-3 is evaluated for accumulation windows ending in December, March, June and September, representing the ends of the main rainfall sub-seasons in Iraq (late autumn, winter, spring and the full wet season), which allows the seasonal evolution of drought and wetness patterns over the country to be.

SPI-3 Dec

SPI-3 (Dec) shows a marked increase in short-term variability with frequent strong drought and wetness events. The period 2007-2008 recorded the lowest significant value (-2.28), while 2018-2019 emerged as the wettest year (+3.58) (Fig. 4). The 5-year moving average reveals alternating cycles between dry and wet conditions, with a rising trend after 2010, suggesting an increase in short-term wet years in the last decade.

SPI-3 Mar

The Mar series (Fig. 4) is less oscillatory than the Dec series, but shows two distinct episodes: the dryness of the late 1980s (1988-1989 about -2.27) and the wetness of 2018-2019 about +2.51. The 5-year moving average shows a gradual transition from slightly negative values in the 1990s to more positive values after 2010, reflecting a relative improvement in late winter/early spring wetness.

SPI-3 Jun

This trajectory exhibits shorter, mostly neutral oscillations, with a wet peak in 1992-1993 of +1.88 and a dry trough in 1988-1989 of -2.08 (Fig. 4). The moving average remains close to zero most of the time with intermittent spikes, indicating Jun's sensitivity to late spring and early summer rainfall changes without a strong long-term trend.

SPI-3 Sept

The Sept panel shows sharp contrast over the last decade, with a notable wet peak in 2021-2022 of +3.42 versus slightly negative years such as 2016-2017 of -0.97 (Fig. 4). The moving average shows a clear increase after 2015, indicating improved late summer wetness in recent years, while annual variability remains high.

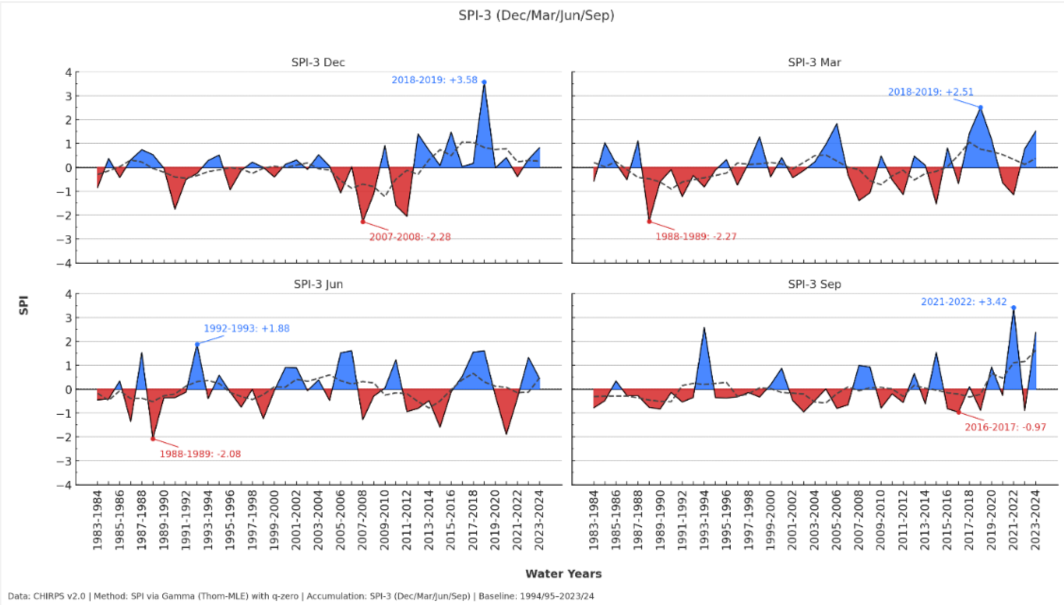

Fig. 4 Temporal variation of the SPI-3 in Iraq at the end of December, March, June, and September, during the water years 1983/84-2023/24. Blue indicates wet periods (positive SPI), red indicates dry periods (negative SPI), and the dark gray dashed line indicates the 5-year moving average, which reflects long-term trends.

4.1.2 Medium-term (SPI-6)

The six-month Standardized Precipitation Index (SPI-6) is designed to quantify precipitation anomalies accumulated over a half-year window, and is therefore more sensitive to seasonal and medium-term water balance than shorter SPI scales. By fitting the six-month precipitation totals to a probability distribution (commonly the gamma distribution) and transforming them to a standard normal variable, SPI-6 expresses deficits and surpluses in units of standard deviation relative to the long-term climatology. Negative SPI-6 values indicate increasing degrees of seasonal drought, while positive values denote seasonal wetness, making this timescale particularly suitable for assessing impacts on soil moisture, streamflow, and reservoir levels over periods of several months (WMO, 2012).

SPI-6 Mar

As a semi-annual index that ends with March, it reflects the impact of the rainfall accumulation over the winter months. 2007-2008 was the most severe drought (-2.11), whereas 2018-2019 the wettest (+3.65) (Fig. 5). Compared to SPI-3 the trajectory seems less erratic, the moving average indicates an overall gradual upward trend after the year 2010, which translates into an improvement of the winter/early spring moisture supply on the medium term.

SPI-6 Sep

This index combines the behaviour of rainfall between the spring and late summer. Significantly 1992-1993 was a year of high wetness (+1.88) in comparison to the dryness in 1988-1989 (-2.09) (Fig. 5). The moving average is still close to neutral, and slightly positive biased during the last decade, indicating a relative improvement of seasonal humidity into the end of summer although negative episodes are still possible.

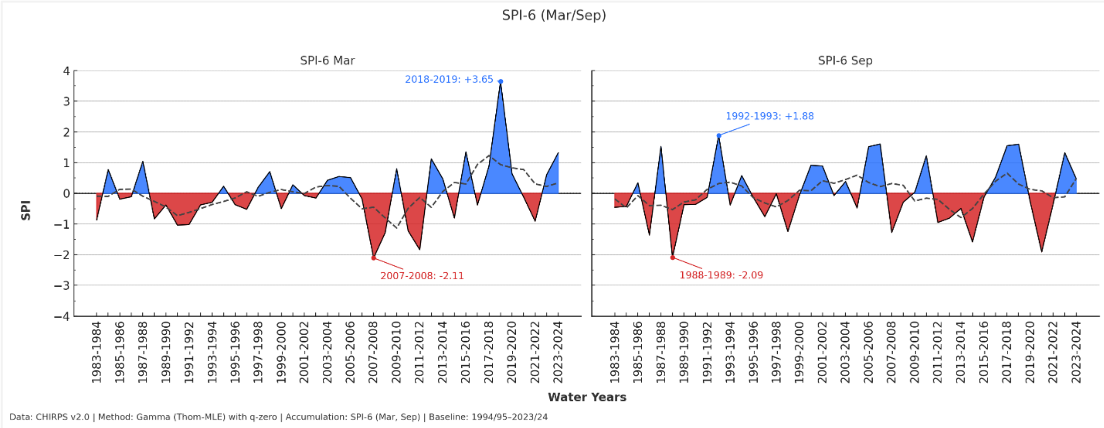

Fig. 5 Temporal variation of the SPI-6 in Iraq at the end of March and September, during the water years 1983/84-2023/24. Blue indicates wet periods (positive SPI), red indicates dry periods (negative SPI), and the dark gray dashed line indicates the 5-year moving average, which reflects long-term trends.

All windows reveal a cyclical oscillation between negative and positive years, with more pronounced extremes after 2000 (large positive peaks in 2018-2019/2021-2022, and significant negative values in 2007-2008 and 1988-1989). The five-year moving average shows a transition from a near-neutral/slightly negative state in the 1990s to a more positive state after 2010, particularly in the December and September windows, suggesting increased humidity variability in the main precipitation seasons.

4.1.2 Long-term (SPI-12 Sep)

The 12-month Standardized Precipitation Index (SPI-12) quantifies anomalies in accumulated precipitation over a full year and therefore reflects long-term hydrological conditions, rather than short-term soil-moisture fluctuations (Guttman, 1999; McKee et al., 1993; WMO, 2012). While short accumulation windows such as SPI-3 are primarily sensitive to seasonal meteorological and agricultural drought, SPI-12 integrates the sequence of wet and dry months across the entire hydrological year and thus is more directly related to changes in groundwater storage, reservoir levels, streamflow and long-term agricultural productivity (Hayes et al., 2011; Mishra & Singh, 2010). Persistent rainfall deficits over several seasons drive SPI-12 to strongly negative values (e.g. below -1.5), signaling severe and extreme hydrological drought, whereas sustained above-normal precipitation pushes SPI-12 into positive ranges, indicating multi-year wet periods that favour aquifer recharge and surface-water recovery. For this reason, SPI-12 is widely recommended as a core index for monitoring prolonged drought events and assessing water-resources vulnerability at basin and national scales (Wilhite & Pulwarty, 2017; WMO, 2012).

The SPI-12 represents the long-term annual rainfall aggregation through September, making it less sensitive to short-term fluctuations and revealing long-term trends. The time series in Fig. 6 shows two distinct phases:

The prolonged dry phase: This was apparent during the late 1980s and has been most pronounced during 2007 and 2008, when the index values were -2.19 (extreme drought), based on an accreted deficit of rainfall over a whole year.

The long-term wet phase: This phase is most prominent after 2010, with the wettest peak in 2018-2019 at +3.52, followed by other positive years close together, indicating a prolonged improvement in humidity rather than a temporary seasonal jump.

The five-year moving average (dashed gray line) indicates a slow change from a negative or near-zero trend during the 1990s and early 2000s to a positive trend after 2010. This kind of behaviour implies that the positive and negative anomalies are no longer alternating with sharp periods as in SPI-3 but rather manifest themselves as relatively continuous (dry/wet) phases over several years. Compared to SPI-3 and SPI-6, SPI-12 peaks are fewer but more indicative of the overall water situation—the high positive/negative number here implies a cumulative surplus/deficit with a direct influence on soil, surface, and groundwater reserves, not simply a single season.

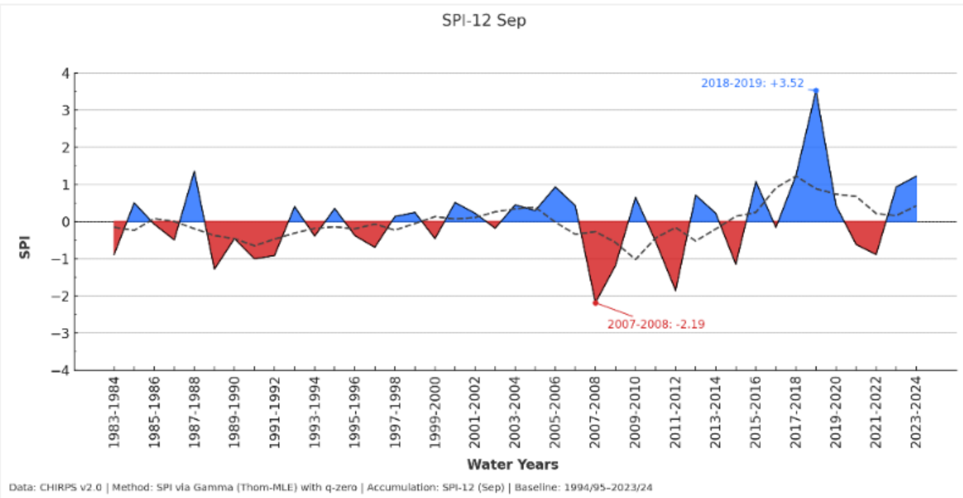

Fig. 6 Temporal variation of the SPI-12 in Iraq at the end of September, during the water years 1983/84-2023/24. Blue indicates wet periods (positive SPI), red indicates dry periods (negative SPI), and the dark gray dashed line indicates the 5-year moving average, which reflects long-term trends.

4.2 Frequency and probability

For the entire period of 41 years of hydrologic record, the frequency table (Table 2) shows that drought and wetness outcomes are mostly confined to the mild categories, with extreme outcomes being relatively rare on either end of the spectrum. For all windows of time, ED and EW outcomes are each at most 2-5%, as expected for the tail of the distribution of an approximately standardized index. By contrast, outcomes of mild drought (ND) and mild wet (NW) are dominant, implying that inter-annual variability is normally small and centered near neutrality, with severe outcomes being episodic.

Table 2 Drought/Wetness Class Frequencies by SPI Windows (41 water year)

Drought Class	SPI-3 Dec	%	SPI-3 Mar	%	SPI-3 Jun	%	SPI-3 Sep	%	SPI-6 Mar	%	SPI-6 Sep	%	SPI-12 Sep	%
Extreme Drought (ED)	2	5	1	2	1	2	0	0	1	2	1	2	1	2
Severe Drought (SD)	2	5	1	2	2	5	0	0	1	2	2	5	1	2
Moderate Drought (MD)	2	5	5	12	3	7	0	0	4	10	3	7	4	10
Mild Drought (ND)	12	29	15	37	19	46	28	68	17	41	19	46	14	34
Mild Wet (NW)	20	49	11	27	8	20	9	22	13	32	8	20	16	39
Moderate Wet (MW)	2	5	5	12	2	5	0	0	4	10	2	5	4	10
Severe Wet (SW)	0	0	2	5	6	15	1	2	0	0	6	15	0	0
Extreme Wet (EW)	1	2	1	2	0	0	3	7	1	2	0	0	1	2

Seasonal contrasts within the SPI-3 windows are pronounced. SPI-3 Dec is skewed toward wetness: NW alone constitutes 49%, with ND at 29%, and only small contributions from MD/MW (each 5%) and the extremes (2-5%). This pattern implies that early-winter totals frequently exceed the long-term median, which is consistent with the pluvial sensitivity of the December window.

Moderate and Mild Wet (MW) add to 24% (12% each) while extreme classes are negligible at 2%. SPI-3 June is the most pronounced bimodal activity of the SPI-3 timescale. While ND continues to be the most common class (46% of observations), a large 15% of observations are in the Severely Wet (SW) class and another 20% in NW. The data indicates that severe three-month pluvial events happen infrequently during late spring yet they possess enough power to qualify as severe events. The SPI-3 Sep index shows a strong preference for dry conditions because its ND value exceeds 68% while it records no severe or moderate drought events and only small amounts of wetness (NW 22% and EW 7% and SW 2%). The ND index reaches its peak in September because dry conditions of late summer season produce standard deficits which stay within acceptable ranges when analyzed through three-month periods.

The six-month accumulations eliminate short-term volatility while maintaining the basic seasonal patterns. The SPI-6 Mar (integrating winter to early spring) shows dry conditions but with moderate intensity: ND 41%, NW 32%, while MD and MW provide 10% each and the remaining areas stay within 2% of extreme values. The SPI-6 Sep structure resembles SPI-3 Jun but it combines data from half of a year: ND 46%, NW 20%, and SW shows a significant 15% value. The spring-to-late-summer period occasionally experiences extended rainy conditions according to the elevated SW share, but the typical weather pattern remains dry.

At the annual scale, SPI-12 (Sep) concentrates most probability near the center: NW is 39% and ND 34%. Moderate categories contribute about 10% each (MD and MW), while extremes remain rare (ED 2%, EW 2%). This distribution is typical for a 12-month standardization: persistent annual deficits or surpluses strong enough to be classified as severe or extreme are infrequent, but when present they are hydrologically consequential. The dominance of ND/NW at SPI-12 underscores that multi-season water-year conditions tend to hover near climatology, with only occasional excursions to the tails.

Taken together, these frequencies imply that managers should plan for frequent mild anomalies and rare but impactful tail events. For SPI-3, operational attention is warranted in June (because of the non-trivial SW share) and September (because of the persistent ND dominance), while December often provides a favorable wet signal. For SPI-6, the September window is the most informative pluvial-risk indicator (given its 15% SW), and for SPI-12 the tails -though scarce-encode multi-season stress or recovery. Translating these shares to implied return periods yields decade-scale or longer recurrences for the severe/extreme classes, while mild conditions recur every two to three years or more often, aligning with the central tendency of a standardized precipitation index over the 41- water year baseline.

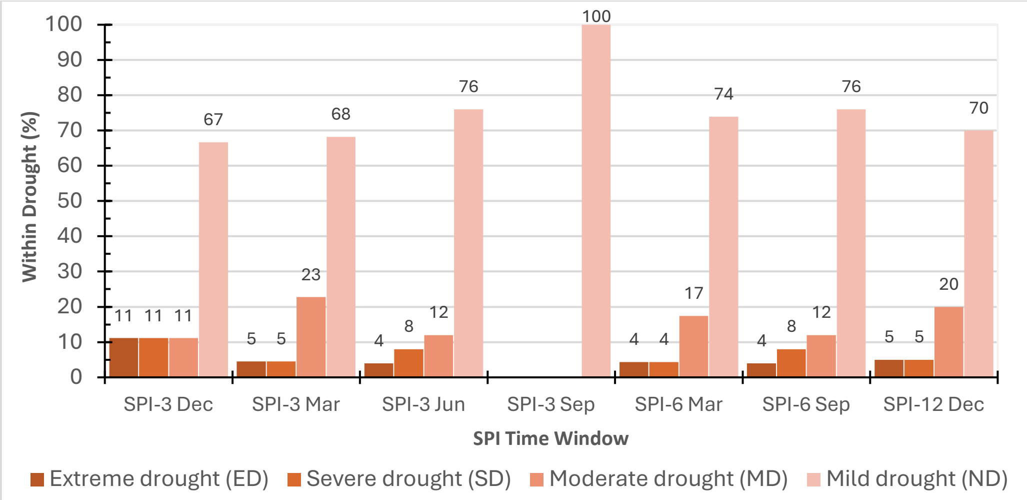

Fig. 7 Conditional frequency of SPI dry-spectrum classes (ED, SD, MD, ND) by end-month for Iraq (water years 1983/84-2023/24). Percentages are computed within drought cases only (ED+SD+MD+ND = 100% per end-month). Windows shown: SPI-3 (Dec/Mar/Jun/Sep), SPI-6 (Mar/Sep), SPI-12 (Dec)

The conditional distribution of SPI dry-severity classes across end-months and time windows (Fig. 7) indicates that drought occurrences are predominantly concentrated in the mild and moderate categories, with severe and extreme drought comprising a small share of drought cases. This structure is consistent with the statistical behavior of a standardized index centered near zero, where probabilities decay toward the tails; hence, the rarer presence of SD and ED relative to ND and MD is theoretically expected and empirically documented for SPI. Moreover, as the accumulation window lengthens from 3 to 6 and 12 months, the distribution tends to "smooth" toward the milder classes because longer integrations average short-lived monthly anomalies and therefore attenuate the frequency of high-magnitude deficits observed at short time scales. This multi-timescale behaviour (inverse relationship between event frequency and timescale and increasing persistence) is in accordance with the original formulation of the SPI as well as later applications (McKee et al., 1993; WMO, 2012).

Inter-end-month differences -for example December, March, June, and September for a 3-months SPI (SPI-3) versus March and September for a 6 - month SPI (SPI - 6), and December only for a 12 - month SPI (SPI-12)- capture seasonal modulation of precipitation regimes: shorter temporal timescale (e.g. SPI-3) are more sensitive to intra - seasonal variability, while longer temporal timescale (e.g. SPI-12) reflect cumulative deficits relevant to storage and longer response components of the hydrological system. Consequently, conditional shares within drought cases commonly shift toward ND (and, to a lesser extent, MD) at longer windows, with SD/ED remaining infrequent. This interpretation is methodologically coherent with SPI's standardization framework and with guidance recommending multi-temporal analysis for monitoring and early warning.(C. Funk et al., 2015; Stagge et al., 2015)

The conditional distribution of SPI wet-severity classes in Fig. 8 shows that wet episodes are dominated by mild (NW) and, secondarily, moderate (MW) categories across most windows, with severe (SW) and extreme (EW) events comprising a comparatively small share of wet cases. For example, NW accounts for 87% at SPI-3 Dec and 72% at SPI-6 Mar (with EW ≤6%), while even at the longest window (SPI-12 Dec) NW remains predominant (76%) and EW is modest (5%). This structure is consistent with the probabilistic behavior of a standardized index centered near zero, for which tail probabilities are intrinsically small; hence, large positive anomalies (SW/EW) appear infrequently relative to mild departures. This expectation is fundamental to SPI's formulation and is reflected in operational guidance recommending interpretation across multiple time scales .

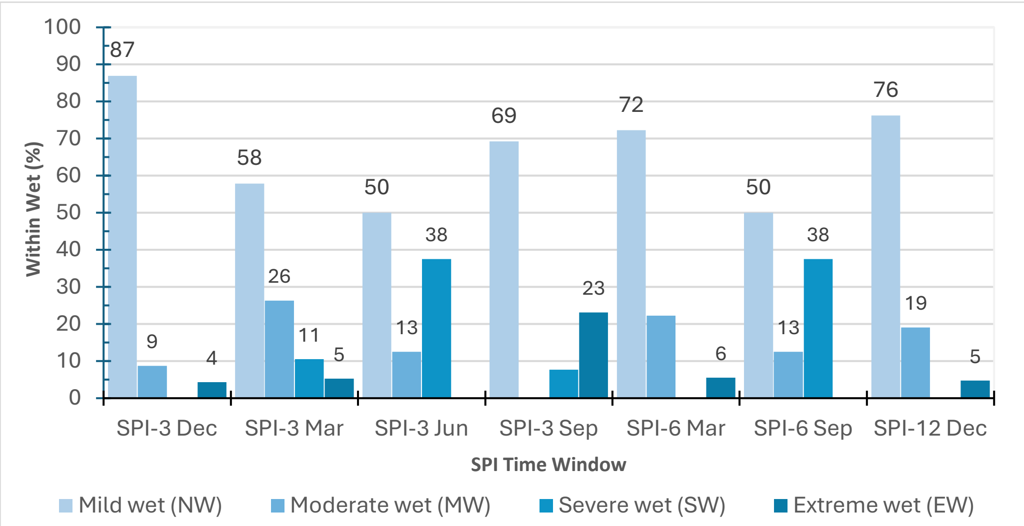

Fig. 8 Conditional frequency of SPI wet-severity classes (NW, MW, SW, EW) by end-month for Iraq (water years 1983/84-2023/24). Percentages are computed within wet classes only (NW + MW + SW + EW = 100% per end-month). Windows shown: SPI-3 (Dec/Mar/Jun/Sep), SPI-6 (Mar/Sep), SPI-12 (Dec).

End-month contrasts highlight seasonal modulation in surplus-producing regimes at short windows and persistence at longer ones. At SPI-3, June stands out with an elevated conditional share of SW = 38% (NW = 50%, EW = 0%), pointing to episodic but intense wet spells during that end-month; conversely, September (SPI-3) shows a notable EW = 23% with MW = 0%, indicating a tail-heavy distribution among wet cases at that scale. By contrast, longer integrations tend to dampen such bursts: at SPI-6 Mar, the distribution shifts toward NW (72%) with SW = 0% and EW = 6%; and at SPI-12 Dec, the conditional shares concentrate in NW/MW (76%/19%) with no SW and only 5% EW. These multi-temporal responses -greater sensitivity to intra-seasonal variability at 3-month windows and aggregation toward milder classes at 6-12 months- agree with the original SPI time-scale framework (frequency decreases and persistence increases with window length) and with best-practice recommendations for multi-scale drought/wetness monitoring.

The threshold–probability analysis (Fig. 9) provides a complementary, distribution-based view of drought and wetness occurrence that is consistent with the time-series patterns shown in Figures 3-5. For each SPI window, we converted the 41-year record into empirical probabilities of crossing commonly used dry-side thresholds (SPI ≤ -1.0, ≤ -1.5, ≤ -2.0) and wet-side thresholds (SPI ≥ +1.0, ≥ +1.5, ≥ +2.0), and quantified sampling uncertainty with two-sided 95% Wilson confidence intervals (Fig. 9). Because all panels share a common y-axis, cross-window comparisons are straightforward: shorter accumulation windows (SPI-3) exhibit larger probabilities for the milder thresholds, whereas longer windows (SPI-6 and SPI-12) suppress short-term noise and yield lower -but hydrologically more consequential- exceedance rates for the severe tails.

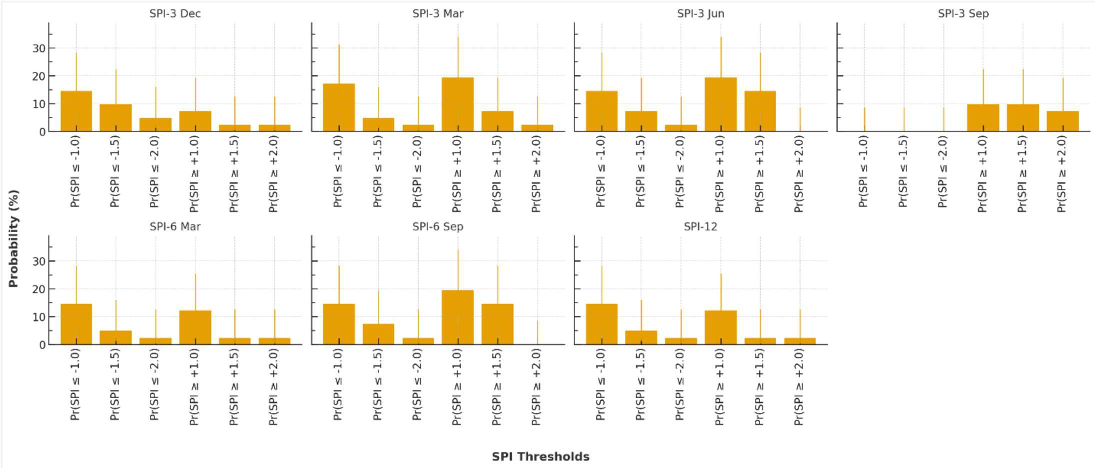

Fig. 9 Threshold probabilities for the Standardized Precipitation Index (SPI) with 95% Wilson confidence intervals. Bars show empirical probabilities (%) for dry-side thresholds (SPI ≤ -1.0, ≤ -1.5, ≤ -2.0) and wet-side thresholds (SPI ≥ +1.0, ≥ +1.5, ≥ +2.0) across the windows: SPI-3 (Dec, Mar, Jun, Sep), SPI-6 (Mar, Sep), and SPI-12 (Sep). Probabilities are computed from 41 water years per window. A common y-axis is used across panels to enable direct comparison.

Seasonal contrasts within SPI-3 are evident. In December, exceedances on the wet side are relatively more likely than in March and June, reflecting the sensitivity of early-winter totals to pluvial anomalies; the Wilson intervals around these probabilities are comparatively narrow, indicating robust estimation from many contributing years. In contrast, the SPI-3 in September is dominated by mild - dry conditions mostly, and very low probabilities of departure from the extreme values, both for severe drought or severe wet conditions, which correspond to the climatological dryness of the late-summer season. June is the middle ground between these two regimes; the probabilities of moderate wetness are not zero - which is to be expected for occasional late spring precipitation bursts - but the distribution in time of these events implies that they are sporadic events rather than regular ones.

When six-month windows are considered, the SPI-6 (Mar) includes the core of the wet season, and therefore has a lower number of threshold crossings compared to the SPI-3 widow. Nevertheless, the threshold crossings that do occur, especially the ones that exceed a +1.5 wetness threshold, have a hydrological significance because they represent half of the water year. SPI-6 (Sep), which aggregates spring through late summer, retains signs of late-season deficits but also captures infrequent pluvial episodes; accordingly, its probabilities are intermediate, with Wilson intervals wider than those of the most common categories but narrower than the tail estimates for SPI-3. In all cases, the uncertainty bands emphasize that apparent differences of a few percentage points between windows should be interpreted cautiously when intervals overlap.

At the annual scale, SPI-12 (Sep) dampens seasonal volatility and concentrates probability mass toward the center of the distribution, producing small but non-zero probabilities for the severe and extreme tails on both sides. The associated Wilson intervals are widest for these rare events -an expected consequence of limited tail samples in a 41-water year record- yet the point estimates still imply practical return periods on the order of decades (roughly one occurrence in 20-50 years for the extreme tails), aligning with expectations for long-memory hydrologic anomalies. Because SPI-12 depicts cumulative water-year circumstances, even low exceedance probabilities have operational weight for multi-season storage, drought recovery, and groundwater recharge.

From a holistic perspective, the probability framing further substantiates the above conclusions that (i) short windows have more variability and seasonality, (ii) the six-month window is a good compromise, and (iii) the annual window is best for summarizing hydrologic steady-state conditions. The 95% Wilson intervals have a dual purpose: they reduce overconfidence in estimates of low-probability events and highlight regions with statistically significant differences between windows. As a result, the discussion in this paper provides a foundation for quantitative likelihoods underlying the time-series plots, making the results immediately applicable for risk-informed decision-making (for example, converting probabilities for ≤ -1.0, ≤ -1.5, and $\geq +1.5$ into suggestive return periods for drought response and wet-year response strategies).

4.3 Spatial Patterns and Areal Extent of SPI-12 Classes over Iraq

To complement the grid-based SPI maps, the areal extent of each drought and wetness category (ND–ED, NW–EW) was quantified for Iraq, following the WMO guidelines on SPI-based drought monitoring, which recommend tracking the fraction of land area falling into each SPI class (WMO & GWP, 2016). For the 12-month SPI ending in September (SPI-12 Sep), which integrates rainfall over the whole water year (October–September) and is therefore most sensitive to long-duration hydrological droughts and pluvial. Table 3 and Fig. 10 show a strong dominance of negative classes over much of the study period, punctuated by a few very wet years.

Across 1983/84–2023/24, mild drought (ND) covers from only about 2,300 km² (0.5%) in 2023/24 up to roughly 354,000 km² (81%) in 1989/90, while moderate drought (MD) ranges from zero in several wet years to about 191,000 km² (44%) in 2008/09. Severe drought (SD) reaches its maximum spatial extent in 2011/12, when about 241,000 km² (55%) of Iraq falls in this class, and extreme drought (ED) peaks in 2007/08, affecting ~70,000 km² (16%). In a number of years – notably 1983/84, 1988/89, 1990/91, 1993/94, 1995/96, 1998/99–1999/2000, 2002/03–2004/05, 2007/08–2008/09 and especially 2011/12 – the combined drought classes (ND+MD+SD+ED) exceed 80–95% of the country, indicating basin-wide, multi-year deficits consistent with hydrological and agricultural drought as defined in the SPI literature .

Table 3 Annual Area of Drought/Wetness Classes in Iraq According to SPI-12 (Sep) of water years 1983/84-2023/24 (km^2)

Water Year	Mild Drought (ND)	Moderate Drought (MD)	Severe Drought (SD)	Extreme Drought (ED)	Mild Wet (NW)	Moderate Wet (MW)	Severe Wet (SW)	Extreme Wet (EW)
1983/84	284,371.02	77,653.81	40,930.58	16,397.32	16,507.44	0	0	0
1984/85	177,694.04	307.18	0	0	212,507.12	32,999.47	7,905.55	4,446.80
1985/86	197,188.26	8,234.68	550.621	0	213,279.43	16,504.66	102.505	0
1986/87	178,230.65	118,686.59	56,643.92	10,361.61	67,569.85	4,168.81	198.734	0
1987/88	155,112.98	34,139.03	521.025	0	51,557.27	39,069.63	75,305.79	80,154.43
1988/89	257,034.64	87,312.39	49,051.18	9,260.93	32,968.70	232.321	0	0
1989/90	354,107.06	15,373.81	3,551.07	352.787	62,475.44	0	0	0
1990/91	269,622.15	100,113.58	22,537.37	1,242.55	42,344.52	0	0	0
1991/92	297,146.68	108,200.09	10,991.28	0	19,522.11	0	0	0
1992/93	158,204.38	15,146.45	930.626	0	199,893.38	55,849.29	5,836.03	0
1993/94	252,823.62	94,821.02	27,457.44	692.709	55,545.88	4,294.11	225.387	0
1994/95	66,246.86	551.225	0	0	303,139.29	64,628.10	1,294.69	0
1995/96	298,051.75	24,114.96	61.673	0	110,083.72	3,548.06	0	0
1996/97	267,436.48	44,283.04	10,237.49	0	107,831.20	5,618.04	453.912	0
1997/98	132,293.06	50.194	0	0	269,855.49	32,521.97	1,139.45	0
1998/99	85,293.83	10,758.76	2,121.57	0	275,319.47	60,251.19	2,115.35	0
1999/2000	264,876.92	26,432.17	15,855.03	3,448.02	125,248.03	0	0	0
2000/01	166,185.94	96.181	0	0	174,809.81	56,093.15	28,028.58	10,646.49

Water Year	Mild Drought (ND)	Moderate Drought (MD)	Severe Drought (SD)	Extreme Drought (ED)	Mild Wet (NW)	Moderate Wet (MW)	Severe Wet (SW)	Extreme Wet (EW)
2001/02	157,072.11	47,422.67	5,516.96	0	164,277.30	29,364.42	27,427.80	4,778.92
2002/03	329,425.45	31,044.96	1,905.75	0	69,377.02	3,866.29	240.688	0
2003/04	54,636.43	0	0	0	350,766.07	30,164.81	292.852	0
2004/05	95,592.34	0	0	0	288,246.23	48,399.68	3,621.91	0
2005/06	23,935.95	81.324	0	0	299,215.21	105,584.02	7,043.65	0
2006/07	79,568.29	0	0	0	349,662.50	6,629.38	0	0
2007/08	49,539.35	136,968.39	179,104.41	70,248.01	0	0	0	0
2008/09	219,318.13	190,564.56	25,493.52	52.32	431.629	0	0	0
2009/10	51,976.78	0	0	0	338,563.89	43,571.35	1,748.15	0
2010/11	281,024.81	83,936.93	8,528.34	0	62,345.42	24.672	0	0
2011/12	16,126.45	147,531.22	241,004.86	31,197.63	0	0	0	0
2012/13	56,002.72	0	0	0	292,665.81	80,738.15	6,453.48	0
2013/14	101,110.33	2,186.53	0	0	230,714.69	94,447.06	7,401.55	0
2014/15	226,048.43	134,249.86	37,538.41	24,635.78	13,372.64	15.045	0	0
2015/16	13,001.01	26.89	0	0	223,211.32	121,509.52	71,905.40	6,206.01
2016/17	248,624.63	19,842.24	3,597.57	184.767	159,728.87	3,882.08	0	0
2017/18	27,195.23	424.613	0	0	225,927.22	109,532.16	66,191.41	6,589.53
2018/19	0	0	0	0	2,721.81	7,255.96	14,088.13	411,794.26
2019/20	196,336.81	11,898.50	555.624	0	205,134.83	17,633.50	4,300.90	0
2021/21	175,237.35	55,634.15	19,221.67	122.283	180,544.17	5,022.57	77.97	0
2021/22	246,727.87	101,961.82	57,878.83	11,525.22	17,766.42	0	0	0
2022/23	55,219.51	6,590.71	0	0	62,234.56	97,474.08	139,777.30	74,564
2023/24	2,260.69	0	0	0	148,752.86	186,369.86	93,334.08	5,142.67

In contrast, wet classes dominate only in a few distinct episodes. The most striking is 2018/19, when drought classes vanish entirely and extreme wetness (EW) covers about 412,000 km² (94.5%), with only small pockets in the milder wet classes. Another strongly pluvial period appears in 2022/23, where wet categories (NW+MW+SW+EW) jointly account for more than 85% of Iraq, and in 2003/04–2006/07 and 2009/10, where near-normal to moderately wet conditions prevail over more than two-thirds of the country. These long-term wet spells likely translate into high river flows and reservoir recharge, whereas the prolonged drought spells around 1998–2001, 2007–2009 and 2011–2012 coincide with well-documented regional drought events over the Fertile Crescent, which severely reduced Tigris–Euphrates flows and agricultural production.

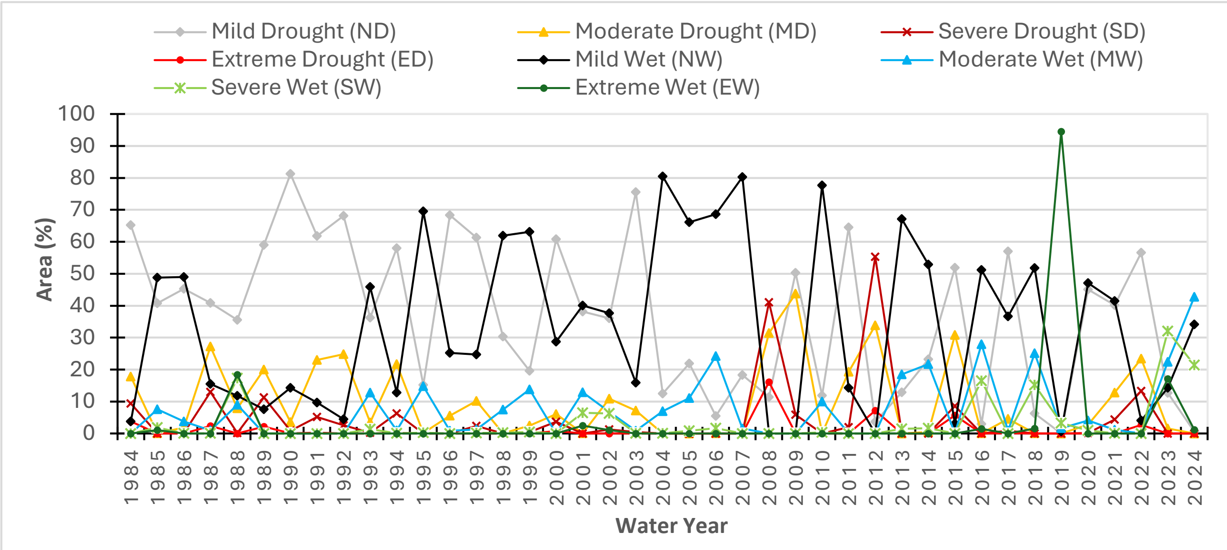

Fig. 10 Annual percentage area of drought and wetness classes in Iraq based on SPI-12 (Sep) for water years 1983/84–2023/24. ND, MD, SD, ED and NW, MW, SW, EW shown as a percentage of Iraq's land area.

Climatically, the prevalence of negative SPI-12 Sep values reflects the strong winter-rainfall regime of Iraq (Hatem et al., 2024). More than 80–90% of annual precipitation in most Iraqi stations falls between November and April, brought by Mediterranean frontal systems and occasional Red Sea troughs, while the extended hot season from late spring to early autumn is almost rain-free and dominated by subtropical subsidence, very high temperatures and frequent Shamal winds that drive potential evapotranspiration to very large values (Hussein, 2024). When one or more consecutive winters are drier than normal, the SPI-6 and SPI-12 indices respond with strongly negative values by late summer and early autumn, because there is no compensating rainfall in summer and soil-moisture and groundwater stores continue to be depleted. This mechanism explains why the 1998/99–1999/2000 and 2007/08–2011/12 periods, which regional studies identify as some of the most intense multi-year droughts in the eastern Mediterranean and Fertile Crescent, appear in SPI-12 Sep series as prolonged intervals where Iraq is almost entirely classified as ND–ED.(Mathbout et al., 2021; Trigo et al., 2010) Conversely, the exceptional wetness of 2018/19 and the pluvial tendency after 2018 reflect one or more very wet winters that raised SPI-12 well above zero, consistent with reports of unusually high seasonal rainfall and widespread flooding in Iraq during those years.

From a drought-monitoring perspective, these SPI-12 Sep results confirm that Iraq is exposed to prolonged, basin-scale droughts roughly once or twice per decade, interspersed with shorter pluvial episodes. According to the standard SPI interpretation, 12-month values integrate both meteorological and hydrological drought, making them suitable for assessing impacts on surface-water resources and long-cycle crops .

The dominance of ND and MD in many years suggests that “mild but widespread” water-stress conditions are very common, while a smaller set of years (e.g. 1983/84, 2007/08, 2011/12) reach truly severe or extreme levels that are consistent with the major drought episodes described in previous work on Iraqi and Fertile Crescent hydro-climate.

Analysis of the drought/wetness frequency map (SPI-12) in Iraq (Fig. 11) shows that all regions of the country experienced a mix of dry and wet years during the period 1983/84–2023/24. The number of years classified as dry per pixel ranged from a minimum of 14 to a maximum of 29 (out of 41 years), while the frequency of wet years ranged from 12 to 27. This means that the wettest area in the country experienced only 14 dry years compared to 27 wet years (this area is approximately 26 km², or ~0.006% of Iraq's total area), while the driest area experienced 29 dry years compared to only 12 wet years (its area is approximately 156 km², or ~0.04%). In general, most of Iraq falls within a medium-frequency range (approximately 18–22 dry years out of 41), with the largest area encompassing about 21 dry years (approximately 102,500 km² or ~23.5% of Iraq's area), corresponding to roughly 20 wet years in the same regions. This medium range is concentrated in the plains of central and southern Iraq. The extreme frequencies are found at the country's geographical peripheries: the driest areas, with the highest drought frequency, are generally located in the desert west and southwest (near the borders with Jordan and Saudi Arabia), where annual rainfall is very low (only ~100–180 mm), while the wettest areas, with the highest frequency of wet years, are located in the mountainous far northeast within the Kurdistan Region bordering Turkey and Iran, where average annual rainfall is high (reaching 300–1000 mm) and drought is less frequent. These findings clearly reflect the climatic gradient in Iraq.

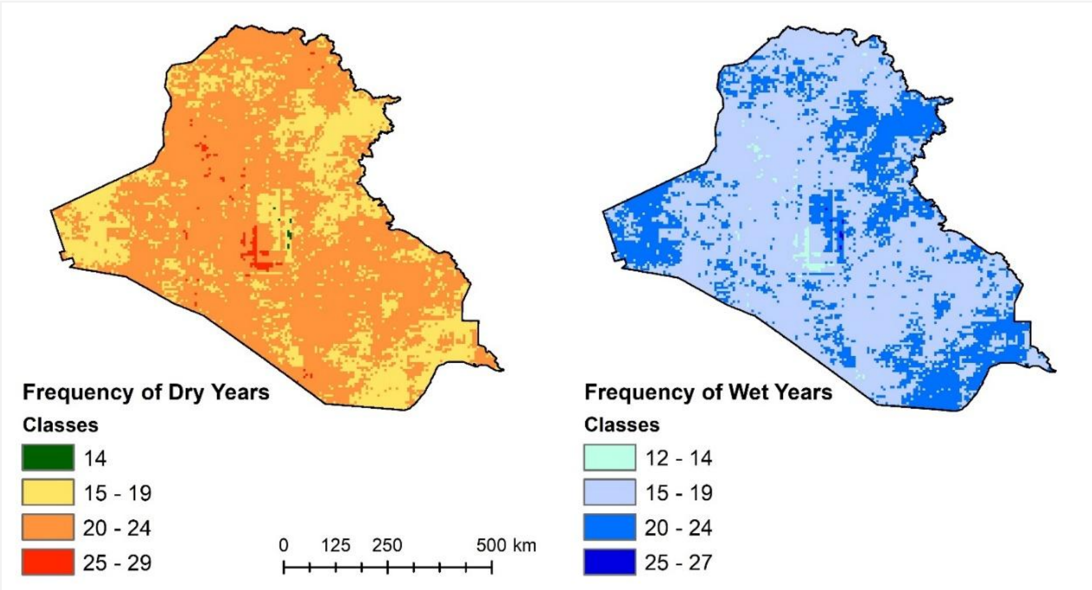

Fig. 11 Spatial distribution of the number of drought/wetness years in Iraq based on SPI-12 (Sep) for water years 1983/84–2023/24. The map on the left shows the prevalence of dry years and the map on the right shows the frequency of years with wet conditions.

5. Conclusion

This study provides a comprehensive and reproducible assessment of meteorological drought dynamics across Iraq by deriving multi-temporal Standardized Precipitation Index (SPI) metrics from satellite-based CHIRPS Daily precipitation data using the Google Earth Engine platformBy adopting a 41-water years baseline (1983/84-2023/24), the analysis captures drought variability across temporal scales and long-term phases at the national level, as well as the frequency of drought and wetness classes.

The results indicate that the drought dynamics of Iraq is of a significantly noticeable interannual variability and a considerable temporal persistence with unique dry and wet regimes that are evident in SPI-3, SPI-6 and SPI-12 timescales. The most evident events of the drought episodes under consideration, based on severity and spatial coherence, were noticednto be in 2007/08 and 2011/12, making these years' events as a national-scale hydroclimatic stress. Conversely, the fiscal year from 2018/19 is oddly associated with wet period representing extended wetness that was evident in all accumulation windows, portraying the enhanced sensitivity of the climate system over Iraq to episodic and large-scale anomalies in circulation.

The short-term standardized precipitation index (SPI-3) was effective to detect the seasonal droughts dynamics and meteorological drought persistence within distinct water years efficiently. Whereas, the medium term SPI-6 displayed the progression of drought and wetness over winter/spring as well as the warm season periods of hydrological cycle. The long-term standardized precipitation index (SPI-12) provided clear evidence of prolonged hydrological drought and recovery phases, linking cumulative precipitation deficits and surpluses to broader water-resources implications.

Methodologically, this study provides validation to the suitability of CHIRPS Daily precipitation data for SPI based drought monitoring in the data-scarce environments and confirms demonstration on the advantage conferred by cloud-based processing in the management of long-term and high resolution climatic datasets.The nationally aggregated framework ensures direct comparability with established SPI applications and aligns with WMO recommendations for standardized drought assessment.

Despite the robustness of the present approach from the methodological point of view, certain uncertainties remain which are related to the sole use of precipitation-based indices and the limited availability of long-term in-situ validation data. Future research should integrate additional hydroclimatic variables, such as evapotranspiration and soil moisture, and explore links between SPI variability and large-scale climate drivers to further refine drought attribution and predictability.

In summary, the present study offers a scientific framework for drought monitoring in Iraq that is robust, operationally feasible, and transferrable and, thus, forms an important basis for early warning systems, water resource planning, and drought adaptation strategies in arid and semi-arid environments.

References

- Abramowitz, M., & Stegun, I. A. (Eds.). (1967). Handbook of Mathematical Functions With Formulas, Graphs, and Mathematical Tables (6th printing, Applied mathematics series, 55). US. Government Printing Office. https://digital.library.unt.edu/ark:/67531/metadc40301/
- AghaKouchak, A., Farahmand, A., Melton, F. S., Teixeira, J., Anderson, M. C., Wardlow, B. D., & Hain, C. R. (2015). Remote sensing of drought: Progress, challenges and opportunities. Reviews of Geophysics, 53(2), 452–480. https://doi.org/10.1002/2014RG000456
- Ahmad, H. Q., Kamaruddin, S. A., Harun, S. B., Al-Ansari, N., Shahid, S., & Jasim, R. M. (2021). Assessment of Spatiotemporal Variability of Meteorological Droughts in Northern Iraq Using Satellite Rainfall Data. KSCE Journal of Civil Engineering, 25(11). https://doi.org/10.1007/s12205-021-2046-x
- Attafi, R., Darvishi Boloorani, A., Fadhil Al-Quraishi, A. M., & Amiraslani, F. (2021). Comparative analysis of NDVI and CHIRPS-based SPI to assess drought impacts on crop yield in Basrah Governorate, Iraq. Caspian Journal of Environmental Sciences, 19(3). https://doi.org/10.22124/cjes.2021.4941
- Degefu, M. A., & Bewket, W. (2023). Drought monitoring performance of global precipitation products in three wet seasons in Ethiopia: Part I—Quasi-objective examination. Meteorological Applications, 30(4). https://doi.org/10.1002/met.2143
- Dejene, I. N., Moisa, M. B., & Gemeda, D. O. (2023). Spatiotemporal monitoring of drought using satellite precipitation products: The case of Borena agro-pastoralists and pastoralists regions, South Ethiopia. Heliyon, 9(3). https://doi.org/10.1016/j.heliyon.2023.e13990
- Dezman, L. E., Shafer, B. A., Simpson, H. D., & Danielson, J. A. (1983). Development of a Surface Water Supply Index — A Drought Severity Indicator for Colorado, in Proceedings Int. Symp. on Hydrometeorology, American Water Resources Association (AWRA), June 13–17, 1982, Colorado, USA, 337–341.
- Funk, C. C., Peterson, P. J., Landsfeld, M. F., Pedreros, D. H., Verdin, J. P., Rowland, J. D., Romero, B. E., Husak, G. J., Michaelsen, J. C., & Verdin, A. P. (2014). A quasi-global precipitation time series for drought monitoring (U.S. Geological Survey Data Series 832). U.S. Geological Survey. https://doi.org/10.3133/ds832
- Funk, C., Michaelsen, J., & Marshall, M. T. (2012). Mapping recent decadal climate variations in precipitation and temperature across eastern Africa and the

sahel. In Remote Sensing of Drought: Innovative Monitoring Approaches. https://doi.org/10.1201/b11863

❖ Funk, C., Peterson, P., Landsfeld, M., Pedreros, D., Verdin, J., Shukla, S., Husak, G., Rowland, J., Harrison, L., Hoell, A., & Michaelsen, J. (2015). The climate hazards infrared precipitation with stations - A new environmental record for monitoring extremes. Scientific Data, 2. https://doi.org/10.1038/sdata.2015.66

❖ Gorelick, N., Hancher, M., Dixon, M., Ilyushchenko, S., Thau, D., & Moore, R. (2017). Google Earth Engine: Planetary-scale geospatial analysis for everyone. Remote Sensing of Environment, 202. https://doi.org/10.1016/j.rse.2017.06.031

❖ Gumus, V. (2023). Evaluating the effect of the SPI and SPEI methods on drought monitoring over Turkey. Journal of Hydrology, 626. https://doi.org/10.1016/j.jhydrol.2023.130386

❖ Guttman, N. B. (1999). Accepting the standardized precipitation index: A calculation algorithm. Journal of the American Water Resources Association, 35(2), 311–322. https://doi.org/10.1111/J.1752-1688.1999.TB03592.X;ISSUE:ISSUE:DOI

❖ Hatem, I., Alwan, I. A., Ziboon, A. R. T., & Kuriqi, A. (2024). Unveiling the persistence of meteorological drought in Iraq: a comprehensive spatiotemporal analysis. Sustainable Water Resources Management 2024 10:5, 10(5), 165-. https://doi.org/10.1007/S40899-024-01145-9

❖ Hayes, M., Svoboda, M., Wall, N., & Widhalm, M. (2011). The lincoln declaration on drought indices: Universal meteorological drought index recommended. Bulletin of the American Meteorological Society, 92(4). https://doi.org/10.1175/2010BAMS3103.1

❖ Hussein, O. G. A. (2024). Determining Rainfall Seasons in Iraq Using the Standardized Precipitation Index (SPI). Journal of the College of Education for Women, 35(3), 47–69. https://doi.org/10.36231/COEDW.V35I3.1749

❖ International Energy Agency (IEA). (2025, January). National Climate Resilience Assessment for Iraq. IEA. Retrieved September 19, 2025, from https://www.iea.org/reports/national-climate-resilience-assessment-for-iraq

❖ Khan, M. M. H., Muhammad, N. S., & El-Shafie, A. (2018). Wavelet-ANN versus ANN-based model for hydrometeorological drought forecasting. Water (Switzerland), 10(8). https://doi.org/10.3390/W10080998

❖ Kim, Y. O., Lee, J. K., & Palmer, R. N. (2012). Etude de prévision de la sécheresse en Corée. Hydrological Sciences Journal, 57(6), 1141–1153. https://doi.org/10.1080/02626667.2012.702212

- Kumanlioglu, A. A. (2020). Characterizing meteorological and hydrological droughts: A case study of the Gediz River Basin, Turkey. Meteorological Applications, 27(1). https://doi.org/10.1002/met.1857
- Liu, S., Wu, Y., Xu, G., Cheng, S., Zhong, Y., & Zhang, Y. (2023). Characterizing the 2022 Extreme Drought Event over the Poyang Lake Basin Using Multiple Satellite Remote Sensing Observations and In Situ Data. Remote Sensing, 15(21). https://doi.org/10.3390/rs15215125
- Mares, C., Mares, I., & Mihailescu, M. (2016). Identification of extreme events using drought indices and their impact on the Danube lower basin discharge. Hydrological Processes, 30(21), 3839–3854. https://doi.org/10.1002/HYP.10895
- Mashuri, Karlina, & Sujono, J. (2025). Assessment of satellite-based rainfall products for drought monitoring in the Siak Watershed, Indonesia. Environmental Challenges, 19, 101134. https://doi.org/10.1016/j.envc.2025.101134
- Mathbout, S., Lopez-Bustins, J. A., Royé, D., & Martin-Vide, J. (2021). Mediterranean-scale drought: Regional datasets for exceptional meteorological drought events during 1975-2019. Atmosphere, 12(8). https://doi.org/10.3390/atmos12080941
- McKee, T. B., Nolan, J., & Kleist, J. (1993). The relationship of drought frequency and duration to time scales. Preprints, Eighth Conf. on Applied Climatology, Amer. Meteor, Soc., January. https://studylib.net/doc/13301994/the--relationship--of--drought--frequency
- Mianabadi, A., Salari, K., & Pourmohamad, Y. (2022). Drought monitoring using the long-term CHIRPS precipitation over Southeastern Iran. Applied Water Science, 12(8). https://doi.org/10.1007/s13201-022-01705-4
- Mishra, A. K., & Singh, V. P. (2010). A review of drought concepts. In Journal of Hydrology (Vol. 391, Issues 1–2). https://doi.org/10.1016/j.jhydrol.2010.07.012
- Mo, X. G., Hu, S., Lin, Z. H., Liu, S. X., & Xia, J. (2017). Impacts of climate change on agricultural water resources and adaptation on the North China Plain. Advances in Climate Change Research, 8(2), 93–98. https://doi.org/10.1016/j.accre.2017.05.007
- Morid, S., Smakhtin, V., & Moghaddasi, M. (2006). Comparison of seven meteorological indices for drought monitoring in Iran. International Journal of Climatology, 26(7), 971–985. https://doi.org/10.1002/JOC.1264
- Mukama, E. B., Yimer, E. A., Mbungu, W. B., Dondeyne, S., & van Griensven, A. (2025). Evaluating the standardized and threshold based drought indices for

historical drought detection in the Great Ruaha River Basin, Tanzania. Natural Hazards, 121(10), 12243–12273. https://doi.org/10.1007/s11069-025-07279-z

- Muthumanickam, D., Kannan, P., Kumaraperumal, R., Natarajan, S., Sivasamy, R., & Poongodi, C. (2011). Drought assessment and monitoring through remote sensing and GIS in western tracts of Tamil Nadu, India. International Journal of Remote Sensing, 32(18), 5157–5176. https://doi.org/10.1080/01431161.2010.494642
- Pálfai, I. (2002). Probability of drought occurrence in Hungary. Quarterly J. Hungarian Meteorological Service, 106(3–4), 265–275. https://scholar.google.com/scholar_lookup?title=Probability%20of%20drought%20occurrence%20in%20Hungary&author=I.%20P%C3%A1lfai&publication_year=2002&pages=265-275
- Palmer, W. C. (1965). Meteorological Drought (Research Paper No. 45). US Department of Commerce, Weather Bureau. https://www.droughtmanagement.info/literature/USWB_Meteorological_Drought_1965.pdf
- Pazhanivelan, S., Geethalakshmi, V., Samykannu, V., Kumaraperumal, R., Kancheti, M., Kaliaperumal, R., Raju, M., & Yadav, M. K. (2023). Evaluation of SPI and Rainfall Departure Based on Multi-Satellite Precipitation Products for Meteorological Drought Monitoring in Tamil Nadu. Water (Switzerland), 15(7). https://doi.org/10.3390/w15071435
- Red Cross Red Crescent Climate Centre (RCCC). (2024, June 29). Country fact sheets II-Iraq. RCCC. Retrieved September 19, 2025, from https://www.climatecentre.org/wp-content/uploads/RCCC-Country-profiles-Iraq_2024_final.pdf
- Salman, S. A., Shahid, S., Afan, H. A., Shiru, M. S., Al-Ansari, N., & Yaseen, Z. M. (2020). Changes in climatic water availability and crop water demand for Iraq region. Sustainability (Switzerland), 12(8). https://doi.org/10.3390/SU12083437
- Shalishe, A., Bhowmick, A., & Elias, K. (2022). Meteorological Drought Monitoring Based on Satellite CHIRPS Product over Gamo Zone, Southern Ethiopia. Advances in Meteorology, 2022, 1–13. https://doi.org/10.1155/2022/9323263
- Stagge, J. H., Tallaksen, L. M., Gudmundsson, L., Van Loon, A. F., & Stahl, K. (2015). Candidate Distributions for Climatological Drought Indices (SPI and SPEI). International Journal of Climatology, 35(13), 4027–4040. https://doi.org/10.1002/JOC.4267

- Suliman, A. H. A., Rajab, J. M., & Shahid, S. (2024). Evaluating the accuracy of APHRODITE and CHIRPS satellite-based Precipitation products for meteorological drought monitoring. Theoretical and Applied Climatology, 155(7), 6567–6579. https://doi.org/10.1007/s00704-024-05015-4
- THOM, H. C. S. (1958). A NOTE ON THE GAMMA DISTRIBUTION. Monthly Weather Review, 86(4), 117–122. https://doi.org/10.1175/1520-0493(1958)086<0117:ANOTGD>2.0.CO;2
- Tigkas, D., Vangelis, H., & Tsakiris, G. (2015). DrinC: a software for drought analysis based on drought indices. Earth Science Informatics, 8(3), 697–709. https://doi.org/10.1007/s12145-014-0178-y
- Trigo, R. M., Gouveia, C. M., & Barriopedro, D. (2010). The intense 2007-2009 drought in the Fertile Crescent: Impacts and associated atmospheric circulation. Agricultural and Forest Meteorology, 150(9). https://doi.org/10.1016/j.agrformet.2010.05.006
- Tsakiris, G., Pangalou, D., & Vangelis, H. (2007). Regional Drought Assessment Based on the Reconnaissance Drought Index (RDI). Water Resources Management, 21(5), 821–833. https://doi.org/10.1007/s11269-006-9105-4
- Tsesmelis, D. E., Leveidioti, I., Karavitis, C. A., Kalogeropoulos, K., Vasilakou, C. G., Tsatsaris, A., & Zervas, E. (2023). Spatiotemporal Application of the Standardized Precipitation Index (SPI) in the Eastern Mediterranean. Climate, 11(5). https://doi.org/10.3390/cli11050095
- Uang-aree, P., Kingpaiboon, S., & Khuanmar, K. (2017). The development of Atmospheric Crop Moisture Index for irrigated agriculture. Russian Meteorology and Hydrology, 42(11), 731–739. https://doi.org/10.3103/S1068373917110073
- UNCCD. (2025). Google Earth Engine Standardized Precipitation Index. United Nations Convention to Combat Desertification. Retrieved September 12, 2025, from https://www.unccd.int/land-and-life/drought/toolbox/google-earth-engine-standardized-precipitation-index?utm_source=chatgpt.com
- UN-SPIDER. (2025). Step by Step: Standardized Precipitation Index (SPI) in Google Earth Engine. United Nations Platform for Space-Based Information for Disaster Management and Emergency Response. Retrieved September 12, 2025, from https://www.un-spider.org/advisory-support/recommended-practices/recommended-practice-drought-monitoring-spi/step-by-step?utm_source=chatgpt.com
- Van-Rooy, M. (1965). A rainfall anomaly index independent of time and space. Notos, 14, 43–48.

- Wei, W., Zhang, H., Zhou, J., Zhou, L., Xie, B., & Li, C. (2021). Drought monitoring in arid and semi-arid region based on multi-satellite datasets in northwest, China. Environmental Science and Pollution Research, 28(37). https://doi.org/10.1007/s11356-021-14122-y
- Wilhite, D. A., & Pulwarty, R. S. (2017). Drought and water crises: Integrating science, management, and policy: Second edition. In Drought and Water Crises: Integrating Science, Management, and Policy, Second Edition. https://doi.org/10.1201/b22009
- World Meteorological Organization (WMO), & Global Water Partnership (GWP). (2016). Handbook of Drought Indicators and Indices (M. Svoboda and B.A. Fuchs). Integrated Drought Management Programme (IDMP). Integrated Drought Management Tools and Guidelines Series 2. Geneva. https://www.droughtmanagement.info/literature/GWP_Handbook_of_Drought_Indicators_and_Indices_2016.pdf
- World Meteorological Organization (WMO). (2012). Standardized Precipitation Index User Guide (M. Svoboda, M. Hayes and D. Wood). (WMO-No. 1090), Geneva. https://www.droughtmanagement.info/literature/WMO_standardized_precipitation_index_user_guide_en_2012.pdf?utm_source=chatgpt.com
- Wu, W., Li, Y., Luo, X., Zhang, Y., Ji, X., & Li, X. (2019). Performance evaluation of the CHIRPS precipitation dataset and its utility in drought monitoring over Yunnan Province, China. Geomatics, Natural Hazards and Risk, 10(1), 2145–2162. https://doi.org/10.1080/19475705.2019.1683082
- Zhang, R., Bento, V. A., Qi, J., Xu, F., Wu, J., Qiu, J., Li, J., Shui, W., & Wang, Q. (2023). The first high spatial resolution multi-scale daily SPI and SPEI raster dataset for drought monitoring and evaluating over China from 1979 to 2018. Big Earth Data, 7(3), 860–885. https://doi.org/10.1080/20964471.2022.2148331
- Zhong, R., Chen, X., Lai, C., Wang, Z., Lian, Y., Yu, H., & Wu, X. (2019). Drought monitoring utility of satellite-based precipitation products across mainland China. Journal of Hydrology, 568. https://doi.org/10.1016/j.jhydrol.2018.10.072